Nano Research
2019, 12(1): 63–68

ISSN 1998-0124 CN 11-5974/O4
https://doi.org/10.1007/s12274-018-2178-6

Research Article

Origin of strong and narrow localized surface plasmon resonance of copper nanocubes

Peng Zheng[1,§], Haibin Tang[1,§], Botong Liu[1,2], Sujan Kasani[1,3], Ling Huang[2] (✉), and Nianqiang Wu[1] (✉)

[1] *Department of Mechanical and Aerospace Engineering, West Virginia University, Morgantown, West Virginia 26506-6106, USA*
[2] *Institute of Advanced Materials, Nanjing Tech University, Nanjing 211816, China*
[3] *Lane Department of Computer Science and Electrical Engineering, West Virginia University, Morgantown, West Virginia 26506, USA*
[§] *Peng Zheng and Haibin Tang contributed equally to this work.*

Received: 8 June 2018 / **Revised:** 15 July 2018 / **Accepted:** 14 August 2018

ABSTRACT

Inexpensive copper nanoparticles are generally thought to possess weak and broad localized surface plasmon resonance (LSPR). The present experimental and theoretical studies show that tailoring the Cu nanoparticle to a cubic shape results in a single intense, narrow, and asymmetric LSPR line shape, which is even superior to round-shaped gold nanoparticles. In this study, the dielectric function of copper is decomposed into an interband transition component and a free-electron component. This allows interband transition-induced plasmon damping to be visualized both spectrally and by surface polarization charges. The results reveal that the LSPR of Cu nanocubes originates from the corner mode as it is spectrally separated from the interband transitions. In addition, the interband transitions lead to severe damping of the local electromagnetic field but the cubic corner LSPR mode survives. Cu nanocubes display an extinction coefficient comparable to the dipole mode of a gold nanosphere with the same volume and show a larger local electromagnetic field enhancement. These results will guide development of inexpensive plasmonic copper-based nanomaterials.

KEYWORDS

copper, nanocube, localized surface plasmon resonance, discrete dipole approximation, interband transition

1 Introduction

Localized surface plasmon resonance (LSPR) is widely utilized in optoelectronics, biosensing, solar energy conversion, photochromics, invisibility cloaks, and other applications [1–6]. Plasmonic materials developed so far are typically made of gold and silver. The relative high cost of gold and silver hinders the commercialization of plasmonic materials. Hence, it is significant to search for low-cost and earth-abundant materials for plasmonic applications. Copper is much less expensive than gold ($0.01/g Cu vs. $40/g Au) [7, 8]. Unfortunately, Cu nanostructures give the impression of weak and broad LSPR bands because of the large imaginary part in their dielectric function [9, 10]. There are at least two factors contributing to the imaginary part of the dielectric function in metals: (i) intrinsic energy loss due to electron collision, and (ii) interband transitions [11, 12]. The intrinsic energy loss can be modeled as a frequency-independent constant for a free-electron-like metal; the influence of interband transitions is delocalized on the frequency scale, but gains strength above a material-dependent energy threshold. Unfortunately, the LSPR band of a Cu nanosphere predicted by the Mie theory shows a large spectral overlap with the interband transitions owing to a low energy threshold at around 2.1 eV, leading to severe plasmon damping [13–15].

Despite an overall large imaginary part in the dielectric function for Cu in the wavelength range from ultraviolet (UV) light through to the near-infrared (NIR) regions, it has been noted that there is a low-loss window between 620 nm (2 eV) and 720 nm (1.72 eV) where the imaginary part significantly drops and becomes comparable to those of Ag and Au. This makes it possible to realize strong plasmon in Cu nanostructures over this narrow spectral window (620–720 nm, or 2–1.72 eV). Van Duyne realized an intense and narrow LSPR peak at 698 nm (1.78 eV) on Cu nanotriangle arrays, which is comparable to the extinction spectral line shape of the Ag and Au nanotriangle arrays with similar dimensions [16]. Sugawa demonstrated an intense LSPR peak at 675 nm (1.84 eV) with the Cu half-shell array [17].

Surprisingly, the experimental results showed that Cu nanocubes displayed an intense LSPR peak with a narrow and asymmetric spectral line shape at around 585 nm (2.12 eV) where interband transitions start to contribute to the energy loss [18–20]. This contradicts the previous understanding that interband transitions strongly damp surface plasmon [14, 21]. It has also been noted that Cu nanocubes exhibit a single LSPR peak whereas Ag nanocubes display multiple peaks that are correlated with different plasmon modes with surface polarization charges at the corners, edges, and facets of the geometry [22–27]. Also, both Cu and Ag nanospheres display a single LSPR peak due to the dipolar plasmon mode, although the LSPR of Cu nanospheres is much weaker than that of their Ag counterparts [19, 28]. These discrepancies suggest that the origin of the single intense LSPR band with a narrow and asymmetric spectral line shape observed in Cu nanocubes may be much different from that of Ag nanocubes, and this demands to be fully understood theoretically.

This study aims to shed light on the origin of the strong and narrow LSPR band of Cu nanocubes. To account for the influence of interband transitions, the dielectric function is decomposed into

Address correspondence to Ling Huang, iamlhuang@njtech.edu.cn; Nianqiang Wu, nick.wu@mail.wvu.edu

a free-electron component and an interband transition component. The plasmon modes are calculated with the discrete dipole approximation (DDA) method for a free-electron-like Cu nanocube and a Cu nanocube under the influence of interband transitions, which suggests that all but one plasmon mode gets damped by the interband transitions. To unravel how interband transitions could interplay with the plasmon modes, a theoretical model is developed. According to this model, a free-electron-like nanocube displays multiple LSPR peaks corresponding to plasmon modes at the corners, edges, and facets. Under the influence of interband transitions, those plasmon modes get damped due to their spectral overlap with interband transitions, inducing a tail of broad background absorption. Only the plasmon mode near or below the threshold of interband transitions survives and maintains a free-electron-like spectral line shape. As a result, the cubic corner mode of a Cu nanocube with the lowest resonance energy near the threshold of interband transitions survives, and it exhibits a distinct, strong, and narrow LSPR peak. In addition, the extinction coefficient and the local electromagnetic field enhancement (EM) are investigated. We believe that the theoretical model developed in this study can be used to study plasmon modes for a nanoparticle of arbitrary shape under the influence of interband transitions, and that this will guide the design of plasmonic nanostructures, especially for inexpensive materials like Cu.

2 Results and discussion

2.1 Optical properties of Cu nanocubes

Figure 1 shows the synthesized Cu nanocubes with a medium edge size of 30 nm (Fig. S1 in the Electronic Supplementary Material (ESM)). The Cu nanocubes, which were suspended in toluene, displayed a single, intense, narrow and asymmetric LSPR peak, as shown with the solid blue curve in Fig. 2. The interband transitions of Cu (shaded light blue region in Fig. 2) exhibited an energy threshold close to the peak wavelength of Cu nanocubes. Surprisingly, the LSPR peak survived the damping by the interband transitions, and even exhibited a distinct asymmetric spectral line shape. The extinction spectrum of a single Cu nanocube with an edge length of 30 nm was also calculated using DDA and plotted with a dashed orange curve in Fig. 2. It displayed a similar spectral line shape consistent with the measurement except for a slightly red-shifted LSPR peak position, which was ascribed to the roundness of the cubic corners [23]. It is noted that the nanocubes used for all calculations in this paper were not rounded to ensure the consistency of data analysis with DDA- and finite-difference time-domain (FDTD)-based numerical simulations and theoretical modeling. The calculation takes 30 nm of edge length for the nanocubes as well as the data of dielectric functions from Johnson and Christy [29] unless specified otherwise.

For the sake of comparison, both Au and Ag nanocubes of the same size were also studied by DDA, as shown in Fig. S2 in the ESM (dashed curves). Rather than displaying a single LSPR peak, a gold nanocube exhibited two peaks slightly separated from each other. A silver nanocube exhibited at least four well-separated peaks. Both of these observations are consistent with previous reports [25, 30]. It is worth noting that interband transitions partially overlap with the plasmon edge for an Au nanocube; but overlap little with the plasmon band for an Ag nanocube, which is in stark contrast to the considerable overlap for a Cu nanocube. This observation strongly suggests that interband transitions play critical and different roles in nanocubes made from different materials.

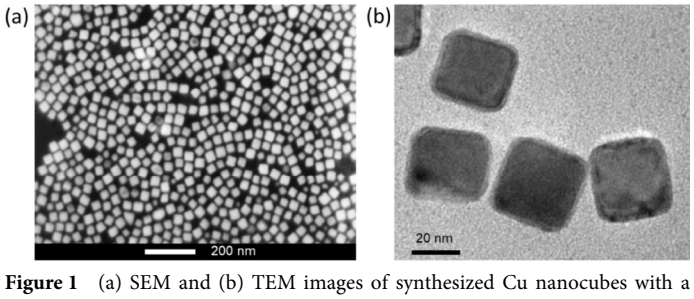

Figure 1 (a) SEM and (b) TEM images of synthesized Cu nanocubes with a medium size of 30 nm (see the size histogram in Fig. S1 in the ESM).

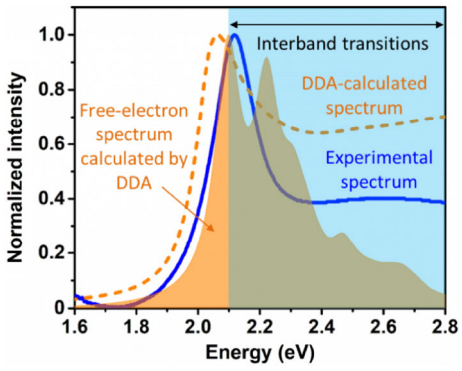

Figure 2 Extinction spectra of measured Cu nanocubes (blue solid curve) and a single Cu nanocube calculated by DDA (dashed orange curve). The orange shaded region shows the extinction spectrum of a free-electron-like (Drude Model) Cu nanocube calculated by DDA. The shaded light blue region shows the interband transitions of Cu.

2.2 Free-electron plasmon modes

To examine what the free-electron-like extinction spectra look like without considering the interband transitions, the dielectric function is decomposed into a free-electron component and an interband transition component [11]. The free-electron component can be modeled using a Drude Model (DM). The DM formula is given by

$$\varepsilon(\omega) = \varepsilon_{\infty} - \frac{\omega_{\mathrm{p}}^2}{\omega^2 + i\gamma\omega} \quad (1)$$

where ε_{∞} is the high frequency permittivity, ω_{p} is the plasma frequency, and γ is the damping constant. The parameters used in the Drude Model for Cu, Au, and Ag were adopted from the literature [22, 31, 32] and tabulated in Table S1 in the ESM. Figure S3 in the ESM shows the free-electron and interband transition components of the dielectric functions for Cu, Au, and Ag. In addition, the calculated free-electron-like extinction spectra for Cu, Au, and Ag nanocubes by DDA are plotted in the orange shaded region in Fig. 2, and Figs. S2(a) and S2(b) in the ESM, respectively. Interestingly, additional plasmon modes were observed in the case of a Cu nanocube (Fig. 2) and an Au nanocube (Fig. S1(a) in the ESM), whereas the Ag nanocube was able to maintain the multiple plasmon modes observed initially regardless of interband transitions, which can be ascribed to the high interband transition energy threshold of Ag. Comparison of DDA-calculated extinction spectra with and without the influence of interband transitions suggests that interband transitions indeed strongly interact with the plasmon modes, which reshape the extinction spectrum of the Cu nanocube. In short, the LSPR peak of Cu nanocubes is affected by the interband transitions rather than the number of plasmonic peaks. A single narrow and asymmetric LSPR peak will occur if there is no damping by the interband transitions.

2.3 Normal modes of a Cu nanocube

Fuchs developed a general approach to calculate the normal modes of nanoparticles of arbitrary shape [33]. When this approach is applied to plasmonic nanostructures, the normal modes refer to surface plasmon modes, which primarily contribute to optical absorption.

For small metallic nanoparticles less than 60 nm (e.g., 30 nm Cu nanocubes), absorption is predominately responsible for extinction. Hence, this study does not distinguish between absorption and extinction while acknowledging the existence of a small contribution from scattering. Following Fuchs's method [33], a theoretical model is adapted herein to provide an insight into the interaction between surface plasmons and interband transitions, and predict the extinction spectrum of a Cu nanocube.

In the subwavelength regime, the retardation effect can be neglected safely. The susceptibility of a nanoparticle is then represented by the sum over all normal modes, which is given by

$$\chi(\omega)=\frac{1}{4\pi}\sum_m\frac{c(m)}{\left(\frac{\varepsilon}{\varepsilon_h}-1\right)^{-1}+n_m},\ \sum_m c(m)=1 \tag{2}$$

where m is the index of normal modes, ε is the dielectric function of the nanoparticle under study, and ε_h is the dielectric constant of the host environment. The normal mode resonance frequencies are determined by the depolarization factor n_m with the absorption strength given by $c(m)$. For a nanosphere under uniform polarization, there is only a single mode thanks to the symmetry of the geometry. The depolarization factor of a nanosphere is $n_m=\frac{1}{3}$, which results in the well-known resonance condition $\frac{\varepsilon}{\varepsilon_h}=-2$ for a dipole mode [13]. For a nanocube, there are at least nine normal modes. However, only six modes have significant strength, accounting for all but 7% of the absorption. The depolarization factors and absorption strengths for the six predominate modes of a nanocube have been previously determined [33]: $n_1=0.193$, $n_2=0.251$, $n_3=0.294$, $n_4=0.396$, $n_5=0.605$, $n_6=0.719$, $c(1)=0.31$, $c(2)=0.31$, $c(3)=0.07$, $c(4)=0.07$, $c(5)=0.13$, and $c(6)=0.04$, with the rest negligible. These modes have surface polarization charges distributed on different parts of the geometry. The first and second modes have the highest amplitudes at the corner, but they have the lowest resonance energy. Therefore, the corner modes can be excited most easily. The fifth and sixth modes have the highest resonance energies with surface polarization charges distributed on the facet, which makes them most difficult to excite.

Based on the susceptibility of a nanoparticle above, the absorption coefficient in the electrostatic approximation can be calculated as follows

$$\alpha(\omega)=4\pi\frac{\omega}{c}\sqrt{\varepsilon_h}VIm\langle\chi(\omega)\rangle \tag{3}$$

where c is the speed of light in vacuum and V is the volume of a Cu nanocube. It is notable that the absorption coefficient is decided by the imaginary part of the susceptibility, which can be calculated by the sum over all six normal modes. Following the Fuchs method, the absorption spectra of a Cu nanocube were calculated using both the measured dielectric function from Johnson and Christy [29] and the free-electron dielectric function fitted by the Drude Model in Eq. (1). The absorption spectra calculated by the Fuchs method were consistent with the results by the DDA method (Fig. 3). For the free-electron-like spectra calculated by both the Fuchs and DDA methods, five out of the six dominant plasmon modes were uncovered with the remaining one beyond the energy range displayed. The plasmon modes, which were overlapping considerably with interband transitions, were significantly broadened and damped except for the one with a resonance frequency near the energy threshold of interband transitions. The calculation by the Fuchs method further underscores the critical role that interband transitions play in reshaping the spectral line shape.

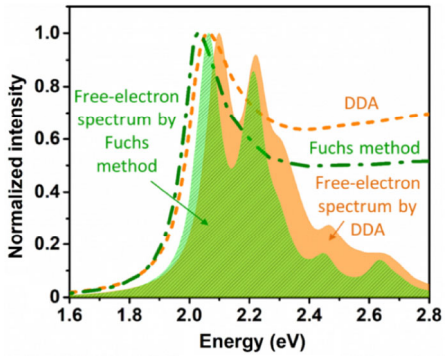

Figure 3 Calculated extinction spectra of a Cu nanocube by Fuchs method (olive color) and DDA method (orange color). The dashed and dash doted curves were calculated using the dielectric function from Johnson and Christy; the shaded data was calculated using a free-electron dielectric function fitted by the Drude Model in Eq. (1). The parameters used in the Drude Model are tabulated in Table S1 in the ESM.

Based on the observations above, we were motivated to understand the mechanism of interaction between interband transitions and surface plasmons from a theoretical perspective. A detailed theoretical discussion can be found in Section S1 in the ESM. Briefly, the dielectric function of Cu in our theoretical model is decomposed into an interband transition component and a free-electron component using Eq. (1); it is presented in Figs. S3(a) and S3(b) in the ESM. The absorption coefficient under the influence of interband transitions was derived in Eq. (S6) in the ESM, where the real and imaginary parts of the interband transition component both contribute to the resonance frequency shift and linewidth broadening. However, because the contribution of the interband transition component to the dielectric function is very small at and below the threshold of interband transitions (Figs. S3(a) and S3(b) in the ESM), the interband transitions just slightly affect the normal modes; and thus they can maintain well their free-electron-like LSPR spectral features. The normal mode resonance frequencies are basically determined by shape-dependent depolarization factors. This is the reason why the LSPR of Cu nanocubes exhibited a free-electron-like extinction peak near the threshold of interband transitions (Figs. 2 and 3). However, interband transitions and surface plasmons come into full play above the threshold of interband transitions where the contribution of the interband transition component to the dielectric function is significant, which considerably broadens and weakens the extinction band, leaving behind a trail of broad background absorption (Figs. 2 and 3).

As the susceptibility $\chi(w)$ in Eq. (2) has a general form, and is applicable to a nanoparticle with an arbitrary shape, it allows the absorption coefficient derived in Eq. (S6) in the ESM to be generalized in the subwavelength regime by parameterizing all the terms

$$\alpha(\omega)=\sum_m c(m)\frac{A_{m1}\omega^5+A_{m2}\omega^4+A_{m3}\omega^3+A_{m4}\omega^2}{(\omega^2-B_{m1}^2)^2+(B_{m2}\omega)^2} \tag{4}$$

where m represents the number of resonances, A_{ms} (s = 1, 2, 3, 4) are coefficients of higher-order polynomials of w, and B_{m1} and B_{m2} determine the resonance frequency and spectral linewidth, respectively. To validate the generalized absorption coefficient, we applied it to fit the measured and DDA-calculated extinction spectra of Cu nanocubes. The generalized formula fits the extinction spectra perfectly (Fig. 4) and allows us to extract the critical parameters, which are otherwise indirectly accessible in the extinction spectra, such as the resonance frequency and linewidth as tabulated in Tables S2–S4 in the ESM. For the Cu nanocubes synthesized, although only one major LSPR peak is observed at the resonance energy w_{res} = 2.12 eV (as shown in Fig. 4(a)), they actually possess multiple plasmon modes, which are damped but can be extracted

from the fitting parameters in Table S2 in the ESM. A similar observation can also be made for the DDA-calculated extinction spectrum in Fig. 4(b) and Table S3 in the ESM. If the influence of interband transitions is removed, those otherwise damped plasmon modes can be recovered by a free-electron-like Cu nanocube, displaying distinct extinction spectral features, as shown in Fig. 4(c). The fitting parameters are tabulated in Table S4 in the ESM. In Fig. 4(c), the two sharp and intense LSPR peaks with the lowest resonance energies are attributed to the most easily excitable corner plasmon modes, whereas a weak LSPR peak with the highest resonance energy originates from the plasmon mode on the cubic facet, which is the most difficult to excite.

As discussed above, the interplay between surface plasmons and interband transitions above the threshold of interband transitions leads to drastic plasmon damping, which can be observed spectrally in Figs. 2 and 3. By calculating the three-dimensional distribution of surface polarization charges on a Cu nanocube using FDTD, interband transition-induced plasmon damping can also be visualized, as shown in Fig. S5 in the ESM. Without the influence of interband transitions, the correlation between each LSPR mode and the distribution of surface polarization charges is well-defined (left column in Fig. S5 in the ESM). Under the influence of interband transitions, surface polarization charges on the cubic edge and facet cannot last. They redistribute on the cubic corner and end up damping the edge and facet modes that spectrally overlap with interband transitions (Figs. 2 and 3). Because the corner mode can be most easily excited given its low resonance energy, it accumulates a large number of surface polarization charges and has the most intense EM field (Fig. S6 in the ESM).

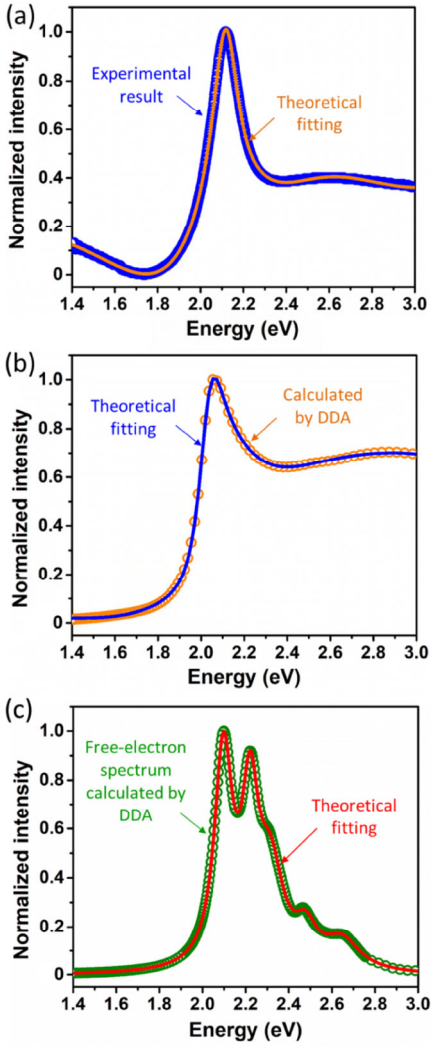

Figure 4 Extinction spectra fitting using the generalized absorption coefficient formula in Eq. (4). (a) Extinction spectrum (thick blue) of synthesized Cu nanocubes and the fitted curve measured with the generalized absorption coefficient formula (orange). (b) Extinction spectrum (orange hollow circles) of a Cu nanocube calculated by DDA and the fitted curve (blue). (c) Extinction spectrum (olive hollow circles) of a free-electron-like Cu nanocube calculated by DDA and the fitted curve (red). The fitting parameters are tabulated in Tables S2 –S4 in the ESM.

2.4 Strong plasmon of a Cu nanocube

From the measured and calculated extinction spectra of Cu nanocubes, the LSPR supported looks much stronger than what could be expected previously from Cu nanospheres. It is interesting to compare the LSPR of Cu nanocubes with those of Au nanocubes and nanospheres to check if a Cu nanostructure is an alternative plasmonic candidate to Au nanostructure. Therefore, the extinction spectrum of a Cu nanocube was calculated using DDA, and compared to those of the Cu nanosphere, Au nanocube, and Au nanosphere (Fig. 5). The nanospheres and nanocubes calculated were modeled to be of the same volume, or equivalently, the same effective radius. Therefore, for a cubic edge length of 30 nm, the spherical diameter used in calculation is about 36 nm. Apparently, the LSPR peak of a Cu nanocube is much stronger and sharper than that of a Cu nanosphere. While it is not as strong as an Au nanocube, it does have an extinction coefficient comparable to that of an Au nanosphere, making it a promising alternative for light management.

Finally, the EM field enhancement factors ($|E|/|E_0|$) for the cubic corner mode of a Cu nanocube was calculated using DDA and compared to the cubic corner mode of an Au nanocube, and the dipole modes of a Cu nanosphere and an Au nanosphere, as shown in Fig. 6. It is evident that the EM field enhancement factor for the cubic corner LSPR mode of a Cu nanocube is less than half that of an Au nanocube, but it is 7.2 times as large as that of a dipole mode of an Au nanosphere. This indicates that Cu nanocubes are alternative plasmonic nanostructures owing to their low cost, comparable extinction coefficient, and large EM field enhancement factor as compared to the Au nanospheres.

3 Conclusions

The LSPR of metallic nanocubes was investigated through experiments, numerical calculation, and theoretical modeling. The theoretical model can be generalized to study the plasmon modes for a nanoparticle of arbitrary shape under the influence of interband transitions in the subwavelength regime, and guide future design of plasmonic nanostructures. In summary, Cu nanospheres generally show a weak and broad LSPR peak due to the severe damping by the interband transitions in the same spectral region of LSPR. In

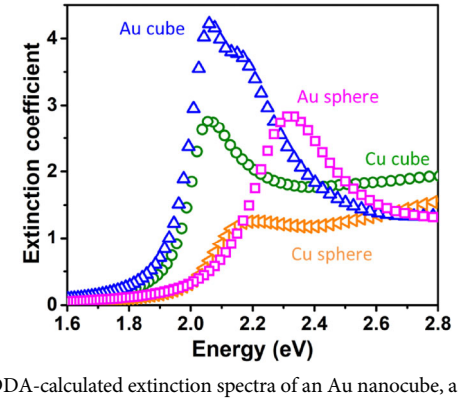

Figure 5 DDA-calculated extinction spectra of an Au nanocube, a Cu nanocube, an Au nanosphere, and a Cu nanosphere. The cubes and spheres calculated are of the same volume, i.e., an edge length of 30 nm for cubes and a diameter of 36 nm for spheres.

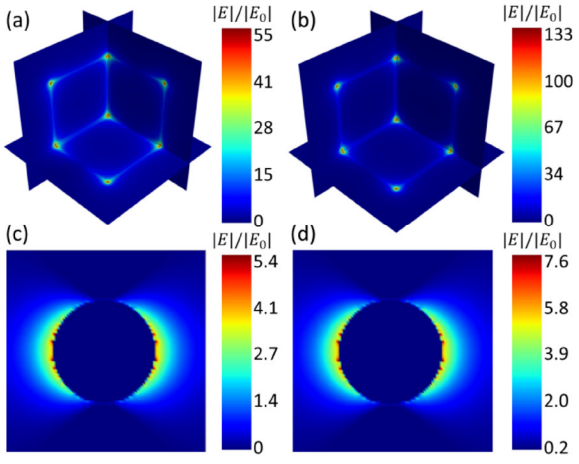

Figure 6 EM field distributions and enhancement factors $|E|/|E_0|$ calculated by DDA for (a) a Cu nanocube, (b) an Au nanocube, (c) a Cu nanosphere, and (d) an Au nanosphere. The peak EM field intensity was used in the calculation of enhancement factor.

contrast, Cu nanocubes exhibit a single strong and narrow LSPR peak. Both numerical and theoretical calculations reveal that the LSPR peak originates from the cubic corner mode, which is also the sole plasmon mode that survives interband transitions-induced damping. By decomposing the dielectric function into a free-electron component and an interband transition component, a free-electron-like Cu nanocube was found to support multiple plasmon modes with surface polarization charges distributed on the corners, edges, and facets of the geometry. Because the cubic corner plasmonic mode has a resonance energy near the threshold of interband transitions, it survives the damping from the interband transitions, maintaining a free-electron-like intense LSPR peak. However, other plasmon modes are spectrally overlapped with interband transitions, and consequently they get dramatically damped, leaving a broad background absorption tilted upward on the higher energy side. In addition, the cubic corner mode of a Cu nanocube contributes to an extinction coefficient that is comparable to that of an Au nanosphere of the same volume and yields a local EM field enhancement factor ($|E|/|E_0|$) that is 7.2 times larger than that of the dipolar LSPR mode. In short, this work demonstrates that Cu nanocubes can be used as cost-effective plasmonic nanostructures.

4 Experimental

4.1 Chemicals and materials

Oleylamine (70%), trioctylphosphine oxide (TOPO, 90%), CuBr, toluene, n-hexane, acetone, and ethanol were purchased from Sigma-Aldrich. All these chemicals were used as received without any further purification.

4.2 Synthesis of Cu nanocubes

Cu nanocubes were synthesized with disproportionation of CuBr [19]. CuBr (0.6 mmol) and TOPO (5 mmol) were dissolved in oleylamine (2 mL) in a three-neck flask with strong magnetic stirring at 80 °C under a nitrogen atmosphere. After 15 min, the resulting solution was rapidly heated to 210 °C and refluxed at this temperature for 1 h before naturally cooling to room temperature. The Cu nanocubes synthesized were separated and washed with hexane for two cycles of centrifugation/redispersion. Finally, Cu nanocubes were dispersed in toluene by ultrasonication for 30 min.

4.3 Characterizations

Synthesized Cu nanocubes were characterized under a JEOL JSM-7600F scanning electron microscope (SEM) and a JEM 2100F transmission electron microscope (TEM) at an acceleration voltage of 200 kV. The extinction spectrum of Cu nanocubes was measured with a Shimadzu 2550 UV-Visible spectrometer (UV 2401/2, Shimadzu).

4.4 DDA calculations

Optical extinction spectra, EM field distributions, and enhancement factors were calculated using the open source code DDSCAT 7.3, developed by Draine et al. [34]. In DDA, the target object is represented by an array of point dipoles. The electromagnetic scattering problem can be solved exactly for an incident wave interacting with these point dipoles. In our study, a total of 125,000 dipoles were used to represent a cubic shape with an edge length of 30 nm. The EM field was extracted at each peak wavelength. All the data for dielectric functions used were from Johnson and Christy [29].

4.5 Electron-driven DDA (e-DDA) calculations

Electron energy loss spectroscopy (EELS) spectra were calculated using open source code e-DDA v1.2 [35], which was compiled based on the DDSCAT code developed by Draine et al. [34]. In our study using e-DDA, swift electron beams with an energy of 300 keV were used to replace the incident light. To excite the corner plasmon mode, we directed the trajectory of incident electrons to pass by the corner of the cube; to excite the facet plasmon mode, which is difficult to excite optically, we directed the trajectory of incident electrons to pass by the facet of the cube.

4.6 FDTD simulation

Surface polarization charge densities were calculated by Lumerical FDTD Solutions 8.15. A total-field scattered-field (TFSF) was used as the input light source. A mesh size of 0.5 nm was used. The dielectric function of Cu was from Johnson and Christy [29]. For a free-electron-like Cu, the dielectric function was fitted using a Drude Model as shown in Eq. (1) with fitting parameters listed in Table S1 in the ESM. The background refractive index was fixed at 1.33. After the plasmon modes of the free-electron-like Cu nanocube were determined by calculating the extinction spectrum, surface polarization charge densities were calculated at the peak wavelength of each mode for both the free-electron-like Cu nanocube and a Cu nanocube under the influence of interband transitions.

Acknowledgements

This work was supported by NIH (R15NS087515). Use of WVU Shared Research Facilities was acknowledged. We are also grateful to the fruitful discussion with Dr. Alexander Govorov at Ohio University.

Electronic Supplementary Material: Supplementary materials (Sections S1–S4, Eqs. (S1)–(S14), Figs. S1–S6, and Tables S1–S4) is available in the online version of this article at https://doi.org/10.1007/s12274-018-2178-6.

References

[1] Du, W.; Wang, T.; Chu, H. S.; Wu, L.; Liu, R. R.; Sun, S.; Phua, W. K.; Wang, L. J.; Tomczak, N.; Nijhuis, C. A. On-chip molecular electronic plasmon sources based on self-assembled monolayer tunnel junctions. *Nat. Photonics* **2016**, *10*, 274–280.

[2] Anker, J. N.; Hall, W. P.; Lyandres, O.; Shah, N. C.; Zhao, J.; Van Duyne, R. P. Biosensing with plasmonic nanosensors. *Nat. Mater.* **2008**, *7*, 442–453.

[3] Andrew, T. L.; Tsai, H. Y.; Menon, R. Confining light to deep subwavelength dimensions to enable optical nanopatterning. *Science* **2009**, *324*, 917–921.

[4] Li, J. T.; Cushing, S. K.; Meng, F. K.; Senty, T. R.; Bristow, A. D.; Wu, N. Q.

Plasmon-induced resonance energy transfer for solar energy conversion. *Nat. Photonics* **2015**, *9*, 601–607.
[5] Ni, X. J.; Wong, Z. J.; Mrejen, M.; Wang, Y.; Zhang, X. An ultrathin invisibility skin cloak for visible light. *Science* **2015**, *349*, 1310–1314.
[6] Gömöry, F.; Solovyov, M.; Šouc, J.; Navau, C.; Prat-Camps, J.; Sanchez, A. Experimental realization of a magnetic cloak. *Science* **2012**, *335*, 1466–1468.
[7] Kawamura, G.; Alvarez, S.; Stewart, I. E.; Catenacci, M.; Chen, Z. F.; Ha, Y. C. Production of oxidation-resistant Cu-based nanoparticles by wire explosion. *Sci. Rep*. **2015**, *5*, 18333.
[8] Gawande, M. B.; Goswami, A.; Felpin, F. X.; Asefa, T.; Huang, X. X.; Silva, R.; Zou, X. X.; Zboril, R.; Varma, R. S. Cu and Cu-based nanoparticles: Synthesis and applications in catalysis. *Chem. Rev*. **2016**, *116*, 3722–3811.
[9] Liu, P. S.; Wang, H.; Li, X. M.; Rui, M. C.; Zeng, H. B. Localized surface plasmon resonance of Cu nanoparticles by laser ablation in liquid media. *RSC Adv*. **2015**, *5*, 79738–79745.
[10] Gunalan, S.; Sivaraj, R.; Venckatesh, R. *Aloe barbadensis Miller* mediated green synthesis of mono-disperse copper oxide nanoparticles: Optical properties. *Spectrochim. Acta Part A: Mol. Biomol. Spectrosc*. **2012**, *97*, 1140–1144.
[11] Pinchuk, A.; Von Plessen, G.; Kreibig, U. Influence of interband electronic transitions on the optical absorption in metallic nanoparticles. *J. Phys. D: Appl. Phys*. **2004**, *37*, 3133–3139.
[12] Khurgin, J. B. Ultimate limit of field confinement by surface plasmon polaritons. *Faraday Discuss*. **2015**, *178*, 109–122.
[13] Zayats, A. V.; Smolyaninov, I. I.; Maradudin, A. A. Nano-optics of surface plasmon polaritons. *Phys. Rep*. **2005**, *408*, 131–314.
[14] Wang, H.; Tam, F.; Grady, N. K.; Halas, N. J. Cu nanoshells: Effects of interband transitions on the nanoparticle plasmon resonance. *J. Phys. Chem. B* **2005**, *109*, 18218–18222.
[15] Dang, T. M. D.; Le, T. T. T.; Fribourg-Blanc, E.; Dang, M. C. The influence of solvents and surfactants on the preparation of copper nanoparticles by a chemical reduction method. *Adv. Nat. Sci: Nanosci. Nanotechnol*. **2011**, *2*, 025004.
[16] Chan, G. H.; Zhao, J.; Hicks, E. M.; Schatz, G. C.; Van Duyne, R. P. Plasmonic properties of copper nanoparticles fabricated by nanosphere lithography. *Nano Lett*. **2007**, *7*, 1947–1952.
[17] Sugawa, K.; Tamura, T.; Tahara, H.; Yamaguchi, D.; Akiyama, T.; Otsuki, J.; Kusaka, Y.; Fukuda, N.; Ushijima, H. Metal-enhanced fluorescence platforms based on plasmonic ordered copper arrays: Wavelength dependence of quenching and enhancement effects. *ACS Nano* **2013**, *7*, 9997–10010.
[18] Yang, H. J.; He, S. Y.; Chen, H. L.; Tuan, H. Y. Monodisperse copper nanocubes: Synthesis, self-assembly, and large-area dense-packed films. *Chem. Mater*. **2014**, *26*, 1785–1793.
[19] Guo, H. Z.; Chen, Y. Z.; Cortie, M. B.; Liu, X.; Xie, Q. S.; Wang, X.; Peng, D. L. Shape-selective formation of monodisperse copper nanospheres and nanocubes via disproportionation reaction route and their optical properties. *J. Phys. Chem. C* **2014**, *118*, 9801–9808.
[20] Crane, C. C.; Wang, F.; Li, J.; Tao, J.; Zhu, Y. M.; Chen, J. Y. Synthesis of copper-silica core-shell nanostructures with sharp and stable localized surface plasmon resonance. *J. Phys. Chem. C* **2017**, *121*, 5684–5692.
[21] Pirzadeh, Z.; Pakizeh, T.; Miljkovic, V.; Langhammer, C.; Dmitriev, A. Plasmon–interband coupling in nickel nanoantennas. *ACS Photonics*, **2014**, *1*, 158–162.
[22] Zhang, S. P.; Bao, K.; Halas, N. J.; Xu, H. X.; Nordlander, P. Substrate-induced Fano resonances of a plasmonic nanocube: A route to increased-sensitivity localized surface plasmon resonance sensors revealed. *Nano Lett*. **2011**, *11*, 1657–1663.
[23] Pellarin, M.; Ramade, J.; Rye, J. M.; Bonnet, C.; Broyer, M.; Lebeault, M. A.; Lermé, J.; Marguet, S.; Navarro, J. R. G.; Cottancin, E. Fano transparency in rounded nanocube dimers induced by gap plasmon coupling. *ACS Nano* **2016**, *10*, 11266–11279.
[24] Ruppin, R. Plasmon frequencies of cube shaped metal clusters. *Z. Phys. D. At., Mol. Clusters* **1996**, *36*, 69–71.
[25] Zhang, K. J.; Da, B.; Ding, Z. J. LSP modes of Ag nanocube and dimer studied by DDA simulation. *Surf. Interface Anal*. **2016**, *48*, 1256–1262.
[26] Cortie, M. B.; Liu, F. G.; Arnold, M. D.; Niidome, Y. Multimode resonances in silver nanocuboids. *Langmuir* **2012**, *28*, 9103–9112.
[27] Mazzucco, S.; Geuquet, N.; Ye, J.; Stéphan, O.; Van Roy, W.; Van Dorpe, P.; Henrard, L.; Kociak, M. Ultralocal modification of surface plasmons properties in silver nanocubes. *Nano Lett*. **2012**, *12*, 1288–1294.
[28] Mogensen, K. B.; Kneipp, K. Size-dependent shifts of plasmon resonance in silver nanoparticle films using controlled dissolution: Monitoring the onset of surface screening effects. *J. Phys. Chem. C* **2014**, *118*, 28075–28083.
[29] Johnson, P. B.; Christy, R. W. Optical constants of the noble metals. *Phys. Rev. B* **1972**, *6*, 4370–4379.
[30] Hooshmand, N.; O'Neil, D.; Asiri, A. M.; El-Sayed, M. Spectroscopy of homo- and heterodimers of silver and gold nanocubes as a function of separation: A DDA simulation. *J. Phys. Chem. A* **2014**, *118*, 8338–8344.
[31] Zeman, E. J.; Schatz, G. C. An accurate electromagnetic theory study of surface enhancement factors for Ag, Au, Cu, Li, Na, Al, Ga, in, Zn, and Cd. *J. Phys. Chem*. **1987**, *91*, 634–643.
[32] Ehrenreich, H.; Philipp, H. R. Optical properties of Ag and Cu. *Phys. Rev*. **1962**, *128*, 1622–1629.
[33] Fuchs, R. Theory of the optical properties of ionic crystal cubes. *Phys. Rev. B* **1975**, *11*, 1732–1740.
[34] Draine, B. T.; Flatau, P. J. Discrete-dipole approximation for scattering calculations. *J. Opt. Soc. Am. A* **1994**, *11*, 1491–1499.
[35] Bigelow, N. W.; Vaschillo, A.; Iberi, V.; Camden, J. P.; Masiello, D. J. Characterization of the electron- and photon-driven plasmonic excitations of metal nanorods. *ACS Nano* **2012**, *6*, 7497–7504.